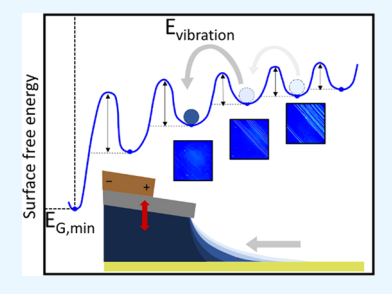
Mitigating Meniscus Instabilities in Solution-Sheared Polymer Films for Organic Field-Effect Transistors

Cecilia Teixeira da Rocha, †,‡ Ge Qu, Xuegeng Yang, Rishi Shivhare, †,‡ Mike Hambsch, †,‡ © Ying Diao, and Stefan C. B. Mannsfeld*, †, ‡ [6]

Supporting Information

ABSTRACT: Semiconducting donor-acceptor copolymers are considered to be a promising material class for solution-coated, large-scale organic electronic applications. A large number of works have shown that the best-performing organic field-effect transistors (OFETs) are obtained on low-surface-energy substrates. The meniscus instabilities that occur when coating on such surfaces considerably limit the effective deposition speeds. This represents a limiting factor for the upscaling of device fabrication for mass production, an issue that needs to be addressed if organic electronic devices are ever to become commercially relevant. In this work, we present a method to increase the accessible window of coating speeds for the solution shearing of donor-acceptor semiconductor polymers for the fabrication of OFETs. By incorporating a piezo crystal



that is capable of producing high-frequency vibrations into the coating head, we are able to mitigate contact line instabilities due to the depinning of the contact line, thereby suppressing the commonly encountered "stick-and-slip" phenomenon.

KEYWORDS: organic field-effect transistors, solution shearing, meniscus instabilities, vibration, large-area fabrication

■ INTRODUCTION

Film instabilities that may occur during solution deposition have been studied but also employed in recent works, most prominently with the intention to precisely control solute deposition to create micropatterned surfaces. 1-7 While the goal may so far have been to exploit the deposition inhomogeneities for gratings and surface patterns, understanding their origin is also of great importance to avoid undesired instabilities such as those appearing during the solution shearing of electronic device films where a continuous and homogeneous film morphology is required.

Several types of patterns have been observed in the literature such as dots, lines, 1-5 and meshes 1,2,6 when colloidal or polymeric systems are solution-sheared. 1,7 These have been described as instabilities that occur at the evaporating contact line of a receding meniscus during solution deposition. 1,8-11 Among these instabilities are Rayleigh dewetting instabilities,¹ stick-and-slip, 1,3,4,12,13 and fingering instabilities. 1,2 Several research groups have investigated the cause and correlation of such patterns to the coating parameters as well as how the combination of multiple instabilities affects the resulting deposited solute. The variables that usually contribute to the occurrence of instabilities are the deposition surface (surface energy and roughness), 1,2,14,15 the concentration of the solute, 1,3,13,16 the solution viscosity, 8 and the deposition speed. 1,4,7

Functionalized surfaces are commonly used for depositing organic semiconductors during the fabrication process of organic field-effect transistors (OFETs). Many past works have shown that especially substrates treated with octadecyltrichlorosilane or octadecyltrimethoxysilane (ODTS) yield better performance for OFETs in general. 17-26 This is usually attributed to either a higher charge carrier density caused by the dipole-induced built-in electrical field from the monolayer, 17,18 an increased molecular ordering, 19-24 or the reduction of electronic trap states as, for example, caused by water. 25 Although it is challenging to cast a uniform film over substrates with low surface energies, ODTS-treated substrates are still preferred over plain SiO₂ substrates when depositing polymer thin films for device fabrication. However, due to the low surface energy of the ODTS-functionalized substrates, dewetting of the solution commonly occurs, leading to meniscus instabilities such as stick-and-slip, especially when solution shearing speeds are increased, and, in extreme cases, the absence of solute deposition on the substrate. The stick-

Received: May 5, 2019 Accepted: July 30, 2019 Published: August 12, 2019

[†]Center for Advancing Electronics Dresden (cfaed) and [‡]Faculty of Electrical and Computer Engineering, Technische Universität Dresden, Helmholtzstraße 18, Dresden 01069, Germany

[§]Department of Chemical and Biomolecular Engineering, University of Illinois Urbana—Champaign, 600 S. Mathews Avenue, Urbana, Illinois 61801, United States

Institute of Fluid Dynamics, Helmholtz-Zentrum Dresden-Rossendorf (HZDR), Bautzner Landstraße 400, Dresden 01328, Germany

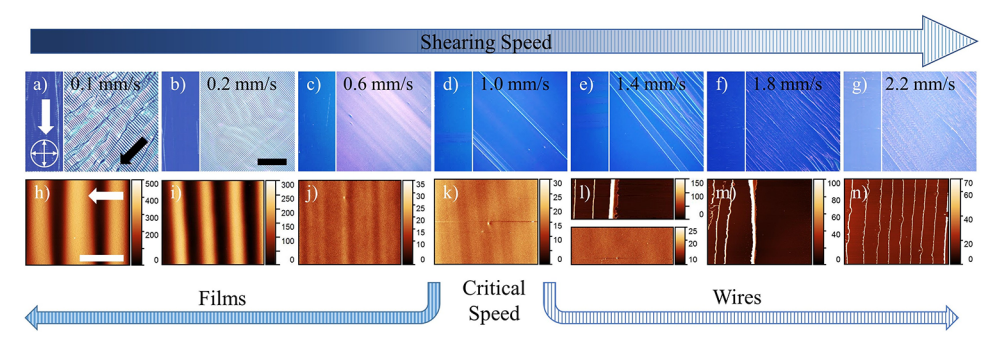


Figure 1. (a–g) Cross-polarized optical microscopy (CPOM) images of films of DPP2T-TT in CF (5 mg/mL), coated at different shearing speeds. Black and white arrows in (a) indicate the solution shearing direction, and the crossed arrows indicate the orientation of the crossed polarizers; these also apply to (a–g). Scale bar in (b), 500 μ m. (h–n) Atomic force microscopy images of the surface of the respective films. Scale bar in (h), 40 μ m. Color bars at the side of AFM images have values given in nanometers.

and-slip instability is thus one of the main obstacles to an increase of the fabrication throughput of polymer-based OFET devices

Stick-and-Slip Behavior in the Solution Shearing of Organic Semiconductor Solutions. The stick-and-slip phenomenon originates from the instability at the contact line of the meniscus, attributed mainly to low-surface-energy substrates that appear incapable of maintaining a prolonged and stable meniscus during the coating process. 12,14,27,28 It is associated with continuous cycles of pinning and depinning of the contact line and has been observed for a diverse range of solutions. ^{1,4,12,13,16,29,30} The pinning—depinning cycles can be described as follows: solvent evaporation at the contact line causes the concentration and the viscosity to increase, pinning the contact line to the substrate when the viscosity exceeds a certain threshold. The pinned contact line subsequently promotes capillary flows toward itself, leading to solute deposition at the pinning point.^{7,16} This deposition of solute at the border of the contact line is commonly termed as the "coffee ring effect". The building pulling force on the meniscus due to the continued motion of the blade eventually leads to depinning and a very fast subsequent slip of the contact line, until it reaches a position closer to equilibrium.

The stick-and-slip phenomenon manifests in thin films as periodic thickness variations and produces films with undulations or "wire" deposits, the latter being a kinetic boundary case of the thickness undulations. When the concentration in the slipping meniscus is too low or the slip speed is too high to adhere to the surface, the result is no film being deposited between the pinning locations, thus forming only "wires". The work of Qu et al. has described the transition from a film to a wire morphology as a result of a shift in the balance between the liquid's surface tension and the interface energy to the substrate that occurs at higher coating speeds. ¹²

Here, we investigate a modification to the solution shearing process that can increase shearing speeds more than two times in comparison to that of the standard method. The shearing speed is raised by stabilization of the contact line that in turn decreases the stick-and-slip effect during the coating process. To achieve this, we embed a vibrational element into the coating head directly attached to the shearing blade. The resulting vibrations that are transduced to the coating liquid reduce the pinning of the meniscus to the substrate, resulting in more continuous films. Through this method, dubbed "piezoshearing", we are able to increase the maximum coating speed, the film uniformity, and the charge carrier mobility of

the films by up to 2 orders of magnitude. In this work, we discuss the use of piezoshearing and its effects on solution-sheared films and OFETs of poly(diketopyrrolopyrrole-cothiophene-co-thiophene-co-thiophene) (DPP2T-TT) and poly[4-(4,4-dihexadecyl-4H-cyclopenta[1,2-b:5,4-b']-dithiophen-2-yl)-alt-[1,2,5]thiadiazolo[3,4-c]pyridine] (PCDTPT). In addition, we provide a more detailed explanation of why more uniform films are obtained.

■ RESULTS AND DISCUSSION

For the following discussion, we first establish the "critical speed" as the lowest speed for which the stick-and-slip instabilities cause the formation of wires instead of a continuous film. ¹² In our experiments, we use a solution concentration of 5 mg/mL of the polymer DPP2T-TT in chloroform and solution-sheared films at room temperature.

Figure 1 shows microscope images of DPP2T-TT sheared at various speeds. For a constant solution concentration, it can be observed that the higher the shearing speed, the more difficult it is to obtain a continuous film. Starting at the shearing speed of 1 mm/s (Figure 1d), we obtain stripes parallel to the contact line, in coexistence with films due to stick-and-slip. The speed of 1 mm/s in this system can then be considered the critical speed.

Mitigation of Contact Line Instabilities through Piezoshearing. While undulations in semiconductor films so far seem not to have been identified as an issue for device fabrication or performance, the formation of wires is a crippling issue for devices that require continuous films and significantly increase device-to-device performance variations. Here, we present a solution that stabilizes the contact line during the solution shearing by subjecting the shearing blade to high-frequency vibrations. We observe that the critical speed for a particular solution concentration is shifted to higher values, resulting in the formation of complete films at shearing speeds that without vibrations would have consisted only of wires. We hypothesize that the vibration introduces enough mechanical energy into the system to constantly "move" the contact line to a state closer to the equilibrium contact line position. In that sense, the additional mechanical energy can be thought of as helping the meniscus to overcome the energetic barrier for unpinning.

The work of Garoff and Decker that investigated a vibrating vertical meniscus provides a very similar description. They found that when introducing energy into the meniscus in the form of vibrations and above a certain threshold it became possible to move the contact line to a lower energy state closer to the minimum global energy contact angle.³²

From the literature, it is also well known that a contact line that has enough defects can be pinned at metastable energy states, which is a cause for contact angle hysteresis.^{33–36} The apparent contact angle can then assume any value between the receding and advancing contact angle, hindering precise characterization of a system's wettability. ^{37,38} If enough energy is injected into the meniscus to overcome the energy barriers that separate these metastable states, the contact line can be moved to a lower energy state, which would be closer to the intrinsic contact angle value. The intrinsic contact angle is considered to be the most stable contact angle, i.e., the position that presents the global energy minimum. 33,41

In addition to discussing a vertical contact line on a plane³² or tube, 39 other previous works have shown that using a large enough vibration amplitude can mitigate contact angle hysteresis in sessile drops. 40,42 This means that vibrations can also be used as a mechanical solution for measuring the most stable contact angle. 37,40,42–45 By studying methods through which one can obtain a contact angle with lower global equilibrium energy, Rodríguez-Valverde et al. have shown that the vibration of water droplets on smooth PDMS surfaces can depin the contact line, resulting in a more stable contact angle, independent of the contact angle of the droplet before vibration. In these experiments, a sine wave function with the resonance frequency of the droplet was used and the amplitude was shown not to be an essential factor, as long as it is over a specific minimum threshold value. 42 The work of Meiron et al. demonstrated that if enough kinetic energy is applied to a sessile drop via vibration, it is possible to depin and move the contact line resulting in a contact angle closer to the most stable contact angle, even on very rough surfaces.³⁷ Additionally, they have shown that if the applied amplitude is too high, the contact line of the drop is deformed.

The evaporation and concentration change at the contact line of our polymer solution can result in higher viscosity and could potentially generate defects at the contact line, increasing the likelihood of the contact line to pin at a position far from the equilibrium for the chosen shearing conditions. As vibrations have been observed to move the contact line in a wide range of works, we believe that the vibrations would also depin the contact line from a metastable position in our receding meniscus setup.

Figure 2 depicts a schematic of our piezoshearing setup. It is the combination of the shear-coater described in previous works^{9,46} and a light-weight silicon shearing blade that is directly attached to a piezo crystal. When an AC voltage is

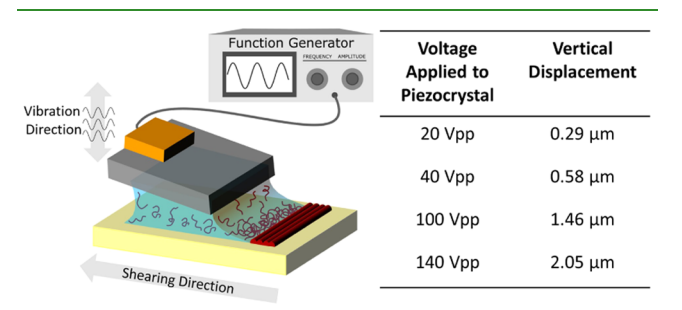


Figure 2. Schematic illustration of the piezoshearing setup and the peak-to-peak voltages applied to the piezo crystal with the equivalent vertical displacement. A constant frequency of 1 kHz was used.

applied to the crystal, it vibrates according to the chosen waveform, frequency, and amplitude. In this study, we use a sinusoidal waveform at a constant vibrating frequency of 1 kHz and peak-to-peak voltages (Vpp) as listed in Figure 2. The voltage applied to the piezo crystal is directly proportional to its displacement. More details regarding the piezoshearing setup can be found in the Experimental Section and in Figures

Next, we compare the effect of the vibration amplitude on the solution shearing of polymer semiconductors by varying the voltage applied to the piezo crystal.

Figure 3 shows the results of piezoshearing deposition of DPP2T-TT (Figure 3u) at different coating speeds using

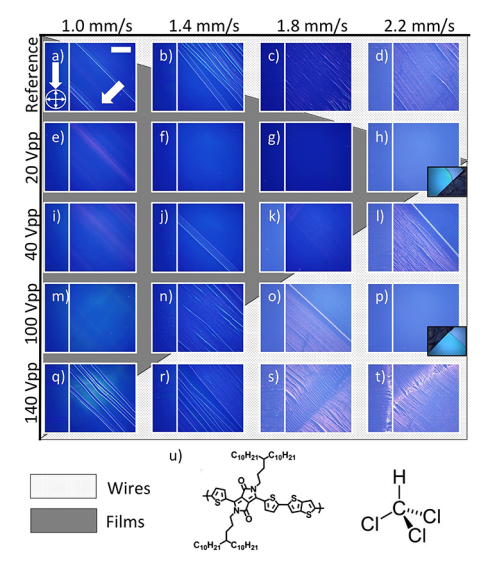


Figure 3. (a-t) CPOM diagram showing films at different shearing speeds and different vibration displacements (constant frequency of 1 kHz). The insets in (h) and (p) are nonpolarized images that show the coating-start region and that are provided to illustrate that despite the uniform colors in (h) and (p) there are indeed thin films. White arrows in (a) indicate the solution shearing direction, and the crossed arrows indicate the orientation of the crossed polarizers. Scale bar: 500 μ m. (u) Chemical structure of DPP2T-TT and chloroform.

different applied voltages for the vibration. AFM images of the various films are shown in Figure S3. The critical speed (transition speed from a film to wire) of the DPP2T-TT polymer in CF is 1 mm/s and can be more than double to over 2 mm/s when utilizing the piezoshearing. At a speed of 2.2 mm/s (Figure 3d), which would provide only wires without vibrations, we can deposit a continuous uniform film (Figure 3h). The films are challenging to image through crosspolarized microscopy due to their very low thickness (down to 7 nm; see AFM results below for evidence that films are indeed formed), which is unusual for sheared films over an ODTS-treated substrate. The insets of Figure 3h,p are optical images of these films.

We also apply the piezoshearing method to the polymer PCDTPT (Figure 4u) to see whether our approach can be applied to polymer semiconductors more generally. We performed the solution shearing of PCDTPT under two different sets of conditions: (i) in chloroform at room temperature and (ii) in chlorobenzene at a substrate temperature of 100 °C. Although the latter conditions resulted in devices with higher charge carrier mobilities, we include the

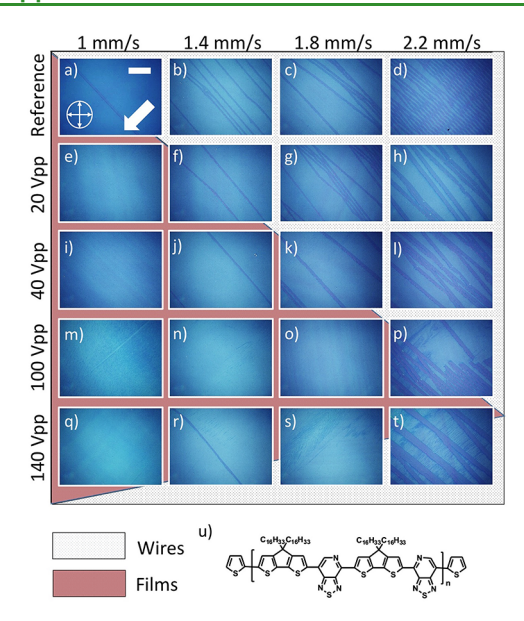


Figure 4. (a–t) CPOM diagram showing films at different shearing speeds and different vibration displacements (constant frequency of 1 kHz). The white arrow in (a) indicates the solution shearing direction, and the crossed arrows indicate the orientation of the crossed polarizers. Scale bar: 500 μ m. (u) Chemical structure of PCDTPT.

experiments with chloroform in our discussion to have a direct comparison to the experiments using DPP2T-TT.

For the shearing of the PCDTPT/CF solution (Figure 4), the critical speed is close to 1 mm/s (Figure 4a), which is similar to DPP2T-TT. The vibration displacement required to yield continuous films is, however, higher than for the DPP2T-TT solution. We attribute this to different capillary characteristics of the meniscus' contact line, requiring different vibration conditions to obtain a continuous film. We consider the capillary number Ca = $\eta V/\sigma_1^{8,47}$ where η is the solution viscosity, V is the shearing speed, and σ is the surface tension of the liquid. Since V is the same for both materials, such capillary number differences can emerge from different viscosity/surface tension ratios. These quantities are inherent to the semiconductor solution and can change due to differences in molecular weight, entanglement, or polymer agglomeration or due to the different surface tension of the polymeric solution in relation to the air and substrate interface. For materials that have a higher number, we would expect the viscosity to predominate over the surface tension factor of the

pinned contact line and therefore require a higher amount of energy (higher displacement of the piezo crystal) to be depinned.

For the PCDTPT/CB (Figure S4) sheared solution, we also observed an improvement in film coverage (reduction of wire formation leads to more uniform coverage) of the deposited films (at speeds of 1.2 and 1.4 mm/s) when the displacement of vibration is large enough. Here, the critical speed is slightly higher, at 1.2 mm/s (Figure S4b). Moreover, the speed gap from the onset of wire occurrence to a wire-only morphology is smaller, meaning the system appears to be more unstable than the CF system. The different capillary characteristics of both systems are likely the reason for this. For the films with speed above the critical speed, full substrate coverage requires a higher displacement for an increased shearing speed. The gradual displacement increase is shown in Figure 4 for the PCDTPT and in a further discussion for DPP2T-TT. It shows that the higher the coating speed, the higher the voltage necessary to mitigate stick-and-slip completely.

In our experiments, we observed that when utilizing piezoshearing, ultralow film thicknesses are attainable; for example, DPP2T-TT film solution-sheared at 2.2 mm/s with a vibration displacement of 20 Vpp reached a thickness of less than 7 nm. In contrast, for films fabricated without vibration. the thinnest films were around 25 nm (Figure S5a). This is a noticeable fact considering that so far only films thicker than 20 nm have been reported for D–A polymers coated on ODTS substrates. ^{12,48–51} For the piezoshearing of PCDTPT/ CF, the lowest thicknesses obtained for a complete film is again 7 nm, while for solution shearing without the vibrations, the minimum thickness is 21 nm (Figure S5b). The films realized by piezoshearing are some of the thinnest films reported for D-A materials for OFET devices and show that our method can successfully improve the adherence of polymer thin films to hydrophobic surfaces. It is worth pointing out that such a reduction in film thickness can not only improve contact resistance 52-56 but also leads to a significant degree of material savings. Especially, modern D-A polymers can still not easily be synthesized in large quantities and therefore represent a significant portion of the total costs of the electronic devices that they are employed in. Reducing the material volume that can generate a continuous film without a reduction in electrical performance is thus a major cost-saving factor.

In the case of the very thin films of DPP2T-TT (thickness \sim 7 nm), such as the one coated at 2.2 mm/s (Figure 3h), it is possible to observe small holes in the film that reach down to

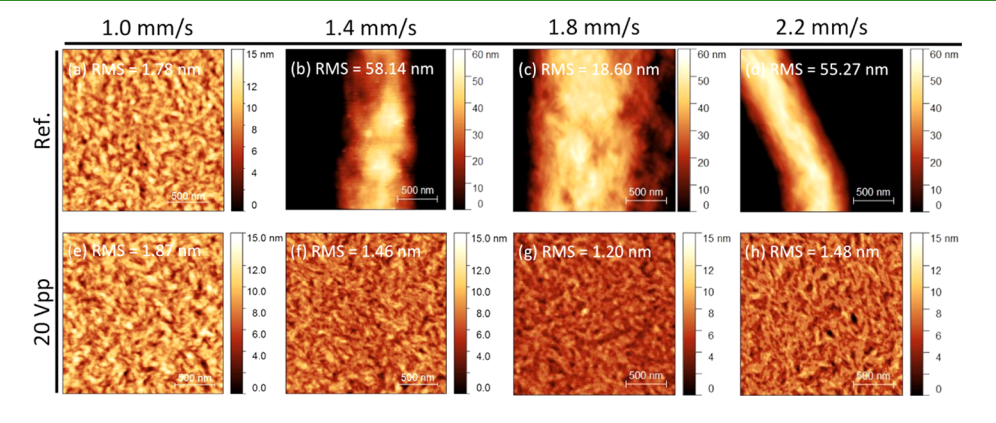


Figure 5. AFM topology for (a-h) solution-sheared films and (e-h) piezosheared films of DPP2T-TT.

ACS Applied Materials & Interfaces

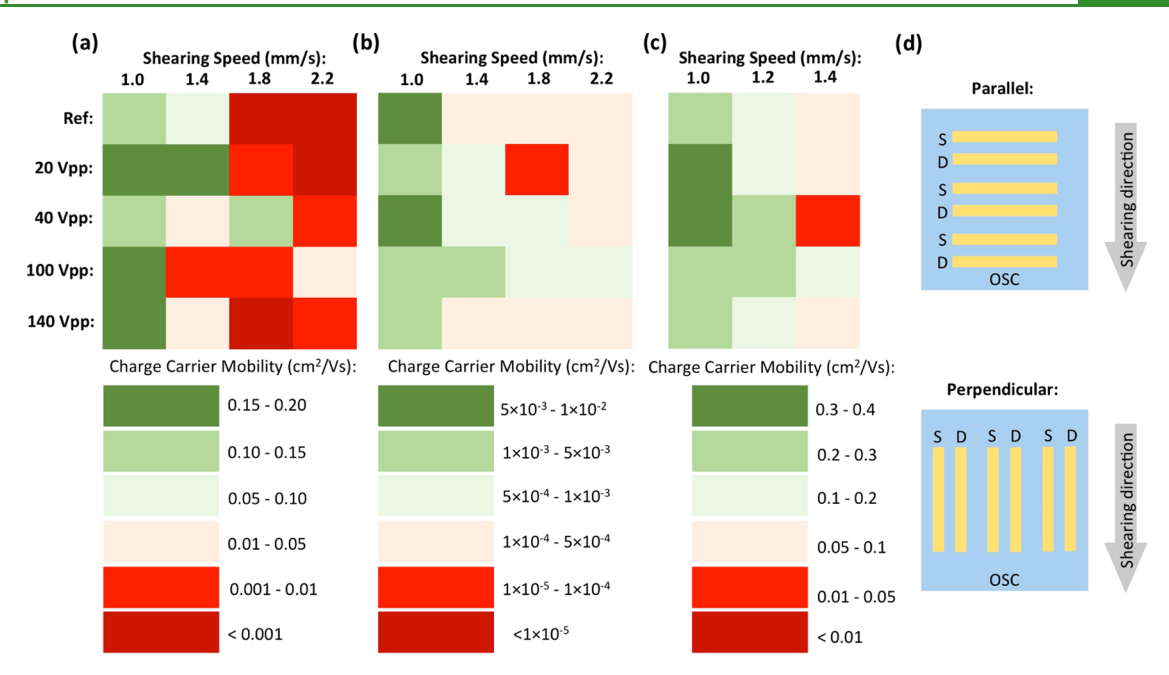


Figure 6. Effective charge carrier mobility values for transistors with transport channel parallel to the shearing direction. Experiments with (a) DPP2T-TT/CF and (b) PCDTPT/CF coated at room temperature and (c) PCDTPT/CB coated at 100 °C. (d) Schematic of OFET electrodes in relation to the solution shearing direction.

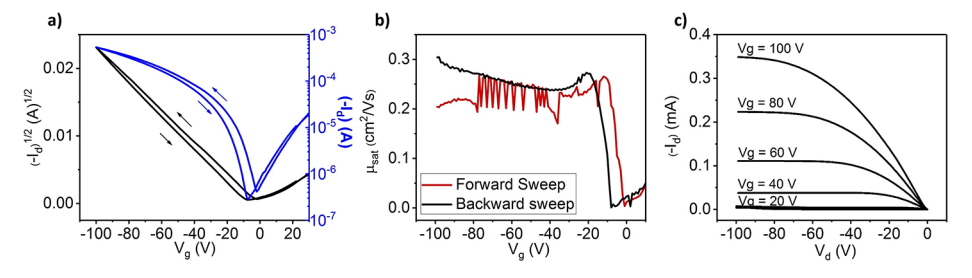


Figure 7. (a) Transfer curves, (b) mobility as function of $V_{g'}$ and (c) output curves for a typical device coated from the polymer DPP2T-TT. The device shown was coated at a speed of 1.0 mm/s and a displacement voltage of 20 Vpp.

the substrate level (Figure 5h). From Figures S5a and S6, we observe that the film thickness as measured from a scratch is similar to the apparent depth of gaps in the film. This means that although the film is completely closed on the macroscale, it might still exhibit some porosity on the microscale.

From Figures 5 and S7, we can gain a detailed view of the surface of the films. Not only is the formation of wires suppressed by piezoshearing, but the degree of polymer agglomeration in fibrils seems to decrease when applying piezoshearing. We can observe from the AFM images (Figure 5f-h) that the piezosheared samples do not present large height variations in the deposit as the ones sheared in the conventional fashion (Figure 5b-d) and display less fibril formation, as observed from phase images in Figure S7. We attribute such fibril formation in the wires to the longer time span the polymer has to aggregate at the contact line while the latter is pinned. The lack of fibril formation for the piezosheared films is consistent with our hypothesis that piezoshearing prevents the contact line from getting pinned.

To check for changes in the molecular packing, we performed grazing-incidence wide-angle X-ray scattering (GIWAXS) parallel and perpendicular to the shearing direction for samples of DPP2T-TT sheared at 1.4 mm/s (above the critical speed). From Figure S8, we observe in all samples a clear peak at 1.74 Å⁻¹ (corresponding to the real

space distance of 3.61 Å), which can be attributed to the $\pi-\pi$ stacking of the polymer backbones, something that is common in conjugated polymers. From this finding, we can conclude that the piezoshearing does not change the $\pi-\pi$ stacking distance of the polymer backbones and thus does likely not impact the polymer chain packing on the nanoscale.

In Figure 6, we present the charge carrier mobility values for devices where the channel direction is parallel to the shearing direction, as schematically shown in Figure 6d, with and without piezoshearing. The values are color-coded in mobility ranges to simplify the observation of a large quantity of data more efficiently. The absolute value for each coating condition is provided in the Supporting Information, Tables S1–S3. For the calculation of average charge carrier mobility values, around five devices were randomly chosen and measured. Both directions, parallel and perpendicular to the shearing direction, were characterized, and the values averaged. Therefore, the charge carrier mobility takes into account both the quality of molecular packing of the films and the coverage of the device's channels.

Due to significantly better coverage of the substrates, we observe that in the films above the critical speed, mobility along the shearing direction can significantly increase, for example, from 6×10^{-4} to 1×10^{-1} cm²/Vs at a coating speed of 1.8 mm/s when applying 40 Vpp to the piezo crystal (Figure

ACS Applied Materials & Interfaces

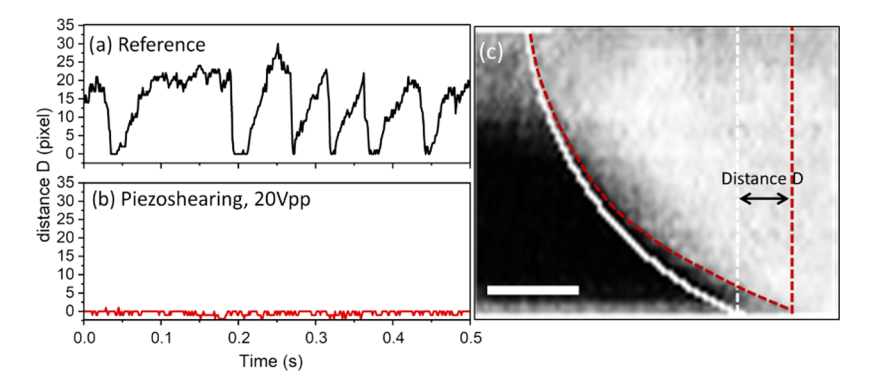


Figure 8. (a) Progress of variation of meniscus edge (distance D in pixels) with shearing over critical speed (1.4 mm/s). (b) Progress of meniscus edge when using piezoshearing. (c) Image of meniscus illustrating how the distance D was calculated; the image was taken during a stick stage. Scale bar in (c): 40 μ m.

6a). We observe mobility improvements for both semiconductor materials in all setups tested. In general, the charge carrier mobility values with vibration are better than the ones without, until the point where the vibration amplitude is too high and makes the contact line more unstable, hindering solute deposition.

In Figure 7, we show typical transfer curves of our DPP2T-TT OFET devices. Due to the occurrence of varying degrees of gate-voltage-dependent mobility, something that is common for many materials with mobilities >0.1 cm²/Vs, ^{59,60} we attempted to report mobility values in the most conservative manner, utilizing the effective mobility as recently defined in the work of Choi et al. 61 The effective charge carrier mobility is the mobility equivalent to an ideal device with the same maximum current value outputted. In this way, overestimations due to gated contact behavior are avoided. 62,63 PCDTPT OFET performance data for both coating setups can be found in Figures S9 and S10.

In the case of charge carrier mobility for devices with the channel perpendicular to the shearing direction, some improvements are observed in Figure S11. It is worth pointing out that for the mobility of devices with the channel in the perpendicular direction, we calculate the total electrode width of the device, and not only the effective electrode width as dictated by the semiconductor wires. Although the piezosheared films (Figure 5f-h) do not exhibit the fibril morphology (Figure 5b-d) that in other cases represents an electrically favorable morphology,¹² the better coverage of the film still produces higher mobility values when considering the full channel width of a device.

Discussion Regarding Improvement on Stick-and-**Slip Instabilities.** To gather visual evidence for the absence of stick-and-slip motion when using the piezoshearing conditions that lead to more continuous films, we attempted to image the stick-and-slip of the meniscus with a microscope camera setup (Video S1) and were able to observe a clear variation in the length of the meniscus. Video S1 shows the meniscus during the shearing of a DPP2T-TT film with a speed of 1.4 mm/s (0.4 mm/s over the critical speed). The white circle approximates the equilibrium meniscus position in all images to serve as a guide to the eye. We observe that during the "stick" position the meniscus is prolonged beyond the white circle. A frame from Video S1 is displayed in Figure 8c. The white line depicts the meniscus front at a position closer to equilibrium as we observe in the video, and the dashed red line shows the stretching of the meniscus during the sticking phase

(Figure S12). When the meniscus "slips", it goes back to overlapping the marked white circle.

For a piezoshearing condition, Video S2, that leads to a continuous film, imaged at the same frame rate, we detect no variation in the shape or length of the meniscus within the resolution of the data. This indicates that there is either no stick-and-slip or that it is either too fast and/or happens on a much smaller length scale than what can be resolved by the camera. To quantify the variation of the position of the meniscus, we measure the distance D (Figure 8c) to which the meniscus stretches beyond the stable meniscus position to compare samples sheared with and without vibration. From Figure 8a, we can observe that the so-defined length of the meniscus increases during the pinning stage (stick stage) and goes back to zero when the slip occurs. In Figure 8b, we observe little or almost no variation in the meniscus length.

Next, we performed an experiment in which we gradually increased the displacement of the piezoshearing for a DPP2T-TT/CF ink to see whether there is an equally gradual decrease in the occurrence of stick-and-slip instabilities. The displacement voltages used in this experiment are much lower than the voltages used for Figure 3. This is done so we can resolve the minimum voltage required to obtain a continuous film in finer detail. In Figure 9, one can see that for constant speed the higher the amplitude of the vibration, the more likely it is to obtain a film free of stick-and-slip instabilities. We also observe this for a drop of drying semiconductor under a static, nonmoving, but vibrating coating blade (Figures S13 and S14). A too low displacement (~2 Vpp) seems not to be enough to mitigate the stick-and-slip, and a too-high displacement (~40 Vpp) seems to hinder any pinning of the contact line, hampering any deposition. This suggests that there might be threshold energy values that need to be overcome to mitigate the stick-and-slip and formation of wires, similar to what is described when moving the contact angle for a sessile drop or a static meniscus with vibration. 32,42 This is in agreement with the work of Decker and Garoff, 32 which relates the moving/ unpinning of the contact line to overcome a local energy barrier to a lower energy state. The energy introduced by the vibrations is proportional to the square of the vibration amplitude (in our case, the piezo crystal's displacement), and thus, overcoming a larger energy barrier requires larger vibration amplitudes.

We also observe that the higher the coating speed, the larger the displacement necessary to obtain a continuous film. Several works associate pinning at metastable positions and contact

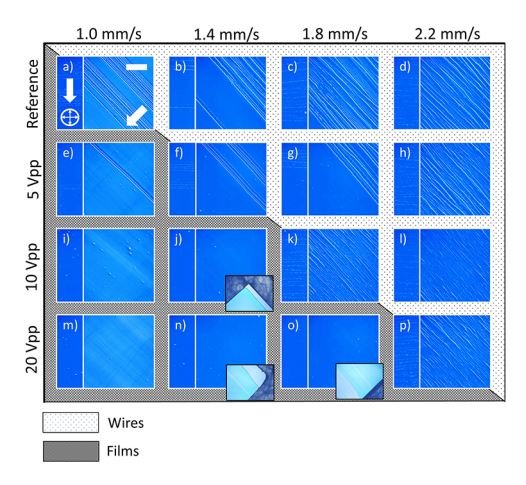


Figure 9. (a-p) Coating of DPP2T-TT at different speeds with increasing vibration displacements, but in a reduced range and with finer steps than in Figure 3. White arrows in (a) indicate the solution shearing direction, and the crossed arrows indicate the orientation of the crossed polarizers. Insets in (j), (n), and (o) display optical images of the ultrathin films.

angle hysteresis to a local energy barrier model, such as the one for metastable states observed in thermal excitation.³ Decker and Garoff³² state that the potential barriers separating the metastable meniscus states depend on their distance from the global equilibrium position and become larger the closer they are to that global equilibrium position. However, in our situation, the moving meniscus represents a force (energy) that constantly acts to stretch the meniscus further away from the equilibrium position and this energy is increasing with the shearing speed. Therefore, at higher shearing speeds (e.g., 2.2 mm/s), the meniscus without vibrations is expected to be at a higher energy state since it is stretched out further than at lower speeds (e.g., 1.0 mm/s) due to viscous forces. 12 To relax to positions near the equilibrium (which is required for constant film deposition), the meniscus requires sufficient additional energy (see Figure 10 for illustration of this hypothesis) to overcome the metastable states separating it from the equilibrium. At higher shearing speeds, the force that

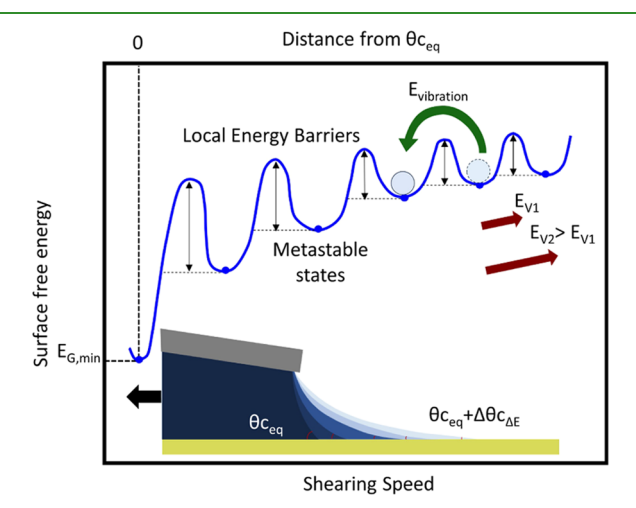


Figure 10. Schematic of a local energy barrier model for the shearing of OSC over the critical speed. The energy introduced by the vibration, $E_{\text{vibration}}$, is counteracted by the kinetic energy of the moving blade, represented by E_{v1} and E_{v2} .

prevents this relaxation is, however, also increasing, depleting the kinetic energy required to rapidly move from the starting meniscus position to the equilibrium position. This is, in our opinion, the reason why with an increasing shearing speed we need an ever-increasing amount of external mechanical energy (vibrations) to allow the meniscus to move rapidly enough to approach equilibrium while the blade motion is constantly countering that relaxation motion.

We demonstrate in this work that it is possible to increase the shearing speed of films sheared for different materials, in different solvents, and at different shearing temperatures. However, the minimum vibration amplitude seems to vary from system to system. This can be explained by different inhomogeneities at the contact line, causing pinning at metastable states to be triggered under different shearing conditions. Such inhomogeneities can arise from nonuniform evaporation at the contact line, ^{33,34} which is not uncommon for polymeric solutions due to agglomeration. 1,8,64 Due to the concentration and viscosity increase in localized regions, "fingers" can emerge, acting as localized defects and anchoring the contact line.⁶⁴ Examples of such finger protuberances can be seen in the AFM images of wires in Figure S15. Surface roughness is also a commonly cited factor that has a significant effect on contact angle hysteresis, 34,35 but due to the ultrasmooth nature of the ODTS substrate in our samples, 24 we believe that it is not the cause of the contact line pinning here. Instead, we speculate that the varying densities and sizes of instabilities along the contact line are also responsible for the different pinning patterns (wire density, etc.).

Regarding heating of the system, we discard the possibility of continuous films due to a heating gradient induced by the piezo crystal. The temperature of the blade when applying the frequency and amplitude parameters used in this work on the piezo crystal was measured and did not rise above room temperature.

CONCLUSION AND OUTLOOK

In this work, we demonstrate the possibility of coating organic semiconductor solutions of donor—acceptor polymers on a hydrophobic substrate with piezo crystal-generated vibrations at higher shearing speeds than would be possible without vibrations with a conventional blade coating setup. We show that the elimination of stick-and-slip effects (Figure 11)

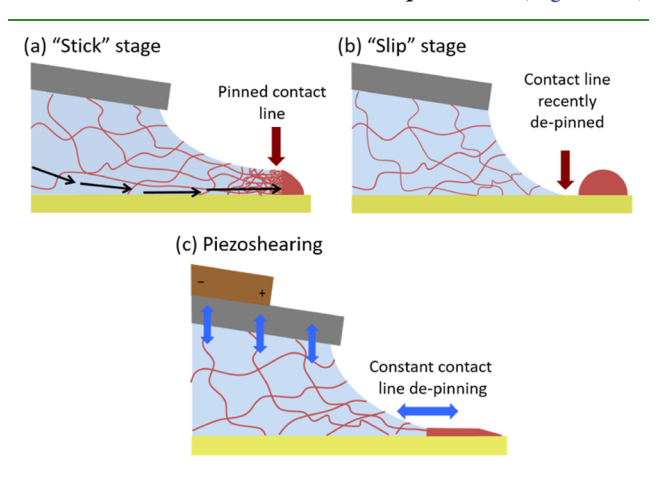


Figure 11. Schematic showing (a) pinning of the contact line (stick), (b) depinning (slip), and (c) constant contact angle due to the vibration of piezoshearing.

produces an increase in the critical shearing speed of over 100% for two different polymer semiconductors and two different solvent-temperature conditions for one of the materials. Furthermore, we show that the charge carrier mobility can increase by 2 orders of magnitude due to better substrate coverage in films coated at increased speeds. We also demonstrate that piezoshearing enables the deposition of ultrathin films in applications in which uniformity and low material consumption are important. Due to the high costs of semiconductor materials and often limited amounts, the reduction of material to a third of the amount used without the vibration represents a significant contribution of the piezoshearing method to fabrication costs.

We believe piezoshearing to be also extendable to other applications that require ultrathin and uniform films, such as dielectrics in ultrathin-film capacitors, transparent electrodes for photovoltaic applications, and strain sensors.

We believe that it is possible to extend this method to different materials and systems that need to be coated at higher speeds on hydrophobic surfaces and still yield good uniformity. It is a simple solution that does not require any changes to the constitution of the deposit or the substrate. We expect this mechanism to be suitable to a wide range of deposition applications by adjusting vibration frequencies and displacement amplitudes to the coating system.

■ EXPERIMENTAL SECTION

Materials. Octadecyltrimethoxysilane was purchased from Sigma-Aldrich. The polymer PCDTPT ($M_w = 75 \text{ kDa}$, PDI = 2.5) was purchased from 1-Material and used without any further purification. The polymer DPP2T-TT ($M_w = 108 \text{ kDa}$, PDI = 6.8) was synthesized following a previously published procedure 65,66 and also used without any further purification.

Piezoshearing Setup. A hydrophobic blade (size 1.6 cm × 1.6 cm) treated with ODTS was used for the piezoshearing assembly. The piezo crystal (model PA4GE, Thorlabs) was attached to an aluminum holder through a temperature-cured epoxy (323LP-T from EPO-TEK). Both the surface of the aluminum holder and the back of the blade were sandpapered to increase abrasiveness of the surface and facilitate adhesion. The aluminum holder was put on a hot plate at 130 °C, and the epoxy was snap-cured with temperature for both the holder-crystal and the crystal-blade bonds, followed by a curing step for 1 h at 130 °C for each bond. After curing, the capacitance of the piezo crystal was remeasured to ensure that there was no damage from heating. The AC voltage was supplied by a waveform generator (60 MHz, Kuman) connected to an AC amplifier (MX200, PiezoDrive), and the output was monitored with an oscilloscope. The same piezo crystal was used for all of the samples described in this manuscript to avoid possible displacement variations between crystals.

Sample Preparation. All samples were fabricated under ambient conditions on highly n-doped silicon wafers with a 300 nm-thick thermally grown SiO₂ layer as a dielectric. The silicon substrates and the shearing blade were treated for hydrophobicity with octadecyltrimethoxysilane (ODTS) according to a method previously published.²⁵ For the polymeric solutions, all materials were dissolved at a concentration of 5 mg/mL in either chloroform or chlorobenzene and stirred at 500 min⁻¹ at 25 °C for at least 2 h before shearing. The substrate temperature was controlled using a thermocouple, and the coating speed was varied utilizing a linear motor from Jenny Science. The blade angle utilized was 8° with a gap of 20 μ m between the edge of the blade and the substrate. For bottom-gate, top-contact transistors, 50 nm-thick Au electrodes were thermally evaporated onto the semiconductor to finish the devices.

Film and Device Characterization. Microscopic images were taken using an optical microscope with a cross polarizer (MOTIC BA310Met). The thickness and surface topography were assessed by

atomic force microscopy using a Nanosurf Flex-Axiom in tapping mode. Thicknesses were measured by gently scratching the thin film down to the substrate and doing an AFM scan perpendicular to the

Grazing-incidence wide-angle X-ray scattering measurements were performed at ID03 surface diffraction beamline of the European Synchrotron Radiation Facility (ESRF), Grenoble. The beam energy for the measurements was 12 keV, and a point detector was used to capture the scattering signal. Two-dimensional reciprocal maps were obtained by stitching together the point detector signal at all of the scattering angles. The grazing-incidence angle for all measurements was 0.12°, and the beam exposure time onto the samples was around 600 s. The 2D scattering data were analyzed using WxDiff software.

All devices were electrically characterized by a Keysight B1500 semiconductor analyzer, and mobilities were calculated from saturation conditions, according to ref 61. The saturation mobility

corresponds to
$$\mu_{\rm sat} = \frac{2L}{WC_{\rm i}} \left(\frac{\partial \sqrt{|{\rm I}_{\rm sd}|}}{\partial V_{\rm g}} \right)^2$$
, derived from the FET saturation

equation. The capacitance used for calculation was 11 nF/cm². The PCDTPT devices were measured under ambient conditions, and the DPP2T-TT devices were measured in air but under a constant flow of nitrogen. For the saturation mobility, the transfer curve $I_{\rm d}{-}V_{\rm g}$ was measured with a $V_{\rm g}$ sweep from 40 to -100 at a constant drain voltage $(V_{\rm d})$ of -100 V. For the output curves $I_{\rm d}{-}V_{\rm d}$, the drain voltage was swept from 0 to -100 V at gate voltages of 0, -20, -40, -60, -80,

High-Speed Imaging. The menisci during solution shearing were imaged using a camera IDT NX4-S1, at a frame rate of 800 FPS, 10× magnification, and frame size of 760×320 pixels. The circles were fit to the menisci using the "Fit Circle" algorithm from Fiji, ImageJ. Fiji was also used to measure the length of the meniscus beyond the fitted

ASSOCIATED CONTENT

Supporting Information

The Supporting Information is available free of charge on the ACS Publications website at DOI: 10.1021/acsami.9b07832.

Piezoshearing setup; AFM images comparing films with and without vibrations; cross-polarized images of the films sheared from PCDTPT/CB; film thicknesses for all materials; cross section of very thin films; AFM phase images comparing films sheared with and without vibration; GIWAXS images and integrated cake sections; tables with compilation of electrical characteristics and electrical curves for devices fabricated from PCDTPT; OFET mobility for devices with active channel perpendicular to shearing direction; still frames from the high-speed imaging experiment; images from the experiment of a drop under vibration; and AFM images of deposits of defects at the contact line (PDF)

Slowed down video for film deposition at 1.4 mm/s without vibration (AVI)

Slowed down video for film deposition at 1.4 mm/s with vibration (AVI)

AUTHOR INFORMATION

Corresponding Author

*E-mail: stefan.mannsfeld@tu-dresden.de.

ORCID ®

Rishi Shivhare: 0000-0001-8519-9415 Mike Hambsch: 0000-0002-8487-0972 Ying Diao: 0000-0002-8984-0051

Stefan C. B. Mannsfeld: 0000-0003-0268-519X

Notes

The authors declare no competing financial interest.

ACKNOWLEDGMENTS

The authors would like to acknowledge support by the German Excellence Initiative via the Cluster of Excellence EXC 1056 "Center for Advancing Electronics Dresden" (cfaed). C.T.d.R. acknowledges financial support from the Center for Advancing Electronics Dresden and the Graduate Academy Dresden. G.Q. and Y.D. acknowledge the US National Science Foundation, NSF DMR Award #18-47828. For the GIWAXS measurements, the authors acknowledge the use of the beamline ID03 (surface diffraction beamline) at the European Synchrotron Radiation Facility (ESRF), Grenoble, France. The authors would like to thank Dr. Linus Pithan for help with setting up the GIWAXS measurements.

■ REFERENCES

- (1) Yabu, H.; Shimomura, M. Preparation of Self-Organized Mesoscale Polymer Patterns on a Solid Substrate: Continuous Pattern Formation from a Receding Meniscus. *Adv. Funct. Mater.* **2005**, *15*, 575–581.
- (2) Liu, Y.; Lee, D. Y.; Monteux, C.; Crosby, A. J. Hyperbranched Polymer Structures via Flexible Blade Flow Coating. *J. Polym. Sci., Part B: Polym. Phys.* **2016**, *54*, 32–37.
- (3) Kim, H. S.; Lee, C. H.; Sudeep, P. K.; Emrick, T.; Crosby, A. J. Nanoparticle Stripes, Grids, and Ribbons Produced by Flow Coating. *Adv. Mater.* **2010**, *22*, 4600–4604.
- (4) Bodiguel, H.; Doumenc, F.; Guerrier, B. Stick—Slip Patterning at Low Capillary Numbers for an Evaporating Colloidal Suspension. *Langmuir* **2010**, *26*, 10758—10763.
- (5) Watanabe, S.; Inukai, K.; Mizuta, S.; Miyahara, M. T. Mechanism for Stripe Pattern Formation on Hydrophilic Surfaces by Using Convective Self-Assembly. *Langmuir* **2009**, 25, 7287–7295.
- (6) Li, S.; Chun, Y. T.; Zhao, S.; Ahn, H.; Ahn, D.; Sohn, J. I.; Xu, Y.; Shrestha, P.; Pivnenko, M.; Chu, D. High-Resolution Patterning of Solution-Processable Materials via Externally Engineered Pinning of Capillary Bridges. *Nat. Commun.* **2018**, *9*, No. 393.
- (7) Thiele, U. Patterned Deposition at Moving Contact Lines. *Adv. Colloid Interface Sci.* **2014**, 206, 399–413.
- (8) Deblais, A.; Harich, R.; Colin, A.; Kellay, H. Taming Contact Line Instability for Pattern Formation. *Nat. Commun.* **2016**, 7, No. 12458.
- (9) Le Berre, M.; Chen, Y.; Baigl, D. From Convective Assembly to Landau—Levich Deposition of Multilayered Phospholipid Films of Controlled Thickness. *Langmuir* **2009**, *25*, 2554–2557.
- (10) Brewer, D. D.; Shibuta, T.; Francis, L.; Kumar, S.; Tsapatsis, M. Coating Process Regimes in Particulate Film Production by Forced-Convection-Assisted Drag-Out. *Langmuir* **2011**, 27, 11660–11670.
- (11) Patel, B. B.; Diao, Y. Multiscale Assembly of Solution-Processed Organic Electronics: The Critical Roles of Confinement, Fluid Flow, and Interfaces. *Nanotechnology* **2018**, *29*, No. 044004.
- (12) Qu, G.; Kwok, J. J.; Mohammadi, E.; Zhang, F.; Diao, Y. Understanding Film-to-Stripe Transition of Conjugated Polymers Driven by Meniscus Instability. *ACS Appl. Mater. Interfaces* **2018**, 40692–40701.
- (13) Byun, M.; Hong, S. W.; Zhu, L.; Lin, Z. Self-Assembling Semicrystalline Polymer into Highly Ordered, Microscopic Concentric Rings by Evaporation. *Langmuir* **2008**, *24*, 3525–3531.
- (14) Shanahan, M. E. R. Simple Theory of "Stick-Slip" Wetting Hysteresis. *Langmuir* 1995, 11, 1041–1043.
- (15) Shanahan, M. E. R. Effects of Surface Flaws on the Wettability of Solids. J. Adhes. Sci. Technol. 1992, 6, 489-501.
- (16) Maheshwari, S.; Zhang, L.; Zhu, Y.; Chang, H.-C. Coupling Between Precipitation and Contact-Line Dynamics: Multiring Stains and Stick-Slip Motion. *Phys. Rev. Lett.* **2008**, *100*, No. 044503.

- (17) Pernstich, K. P.; Haas, S.; Oberhoff, D.; Goldmann, C.; Gundlach, D. J.; Batlogg, B.; Rashid, A. N.; Schitter, G. Threshold Voltage Shift in Organic Field Effect Transistors by Dipole Monolayers on the Gate Insulator. *J. Appl. Phys.* **2004**, *96*, 6431–6438
- (18) Kobayashi, S.; Nishikawa, T.; Takenobu, T.; Mori, S.; Shimoda, T.; Mitani, T.; Shimotani, H.; Yoshimoto, N.; Ogawa, S.; Iwasa, Y. Control of Carrier Density by Self-Assembled Monolayers in Organic Field-Effect Transistors. *Nat. Mater.* **2004**, *3*, 317–322.
- (19) Hambsch, M.; Erdmann, T.; Chew, A. R.; Bernstorff, S.; Salleo, A.; Kiriy, A.; Voit, B.; Mannsfeld, S. C. B. Increased Charge Carrier Mobility and Molecular Packing of a Solution Sheared Diketopyrrolopyrrole-Based Donor—Acceptor Copolymer by Alkyl Side Chain Modification. *J. Mater. Chem. C* **2019**, 3665–3674.
- (20) Chew, A. R.; Ghosh, R.; Pakhnyuk, V.; Onorato, J.; Davidson, E. C.; Segalman, R. A.; Luscombe, C. K.; Spano, F. C.; Salleo, A. Unraveling the Effect of Conformational and Electronic Disorder in the Charge Transport Processes of Semiconducting Polymers. *Adv. Funct. Mater.* **2018**, *28*, No. 1804142.
- (21) Zhang, F.; Mohammadi, E.; Luo, X.; Strzalka, J.; Mei, J.; Diao, Y. Critical Role of Surface Energy in Guiding Crystallization of Solution-Coated Conjugated Polymer Thin Films. *Langmuir* **2017**, 1109–1122.
- (22) Um, H. A.; Shin, J.; Lee, T. W.; Cho, M. J.; Choi, D. H. Modulation of Carrier Mobility of Diketopyrrolopyrrole and Quaterthiophene Containing Copolymer with Self-Assembled Monolayers on Gate Dielectrics of Thin Film Transistors. *Synth. Met.* **2013**, 184, 61–67.
- (23) Virkar, A.; Mannsfeld, S.; Oh, J. H.; Toney, M. F.; Tan, Y. H.; Liu, G.; Scott, J. C.; Miller, R.; Bao, Z. The Role of OTS Density on Pentacene and C ₆₀ Nucleation, Thin Film Growth, and Transistor Performance. *Adv. Funct. Mater.* **2009**, *19*, 1962–1970.
- (24) Ito, Y.; Virkar, A. A.; Mannsfeld, S.; Oh, J. H.; Toney, M.; Locklin, J.; Bao, Z. Crystalline Ultrasmooth Self-Assembled Monolayers of Alkylsilanes for Organic Field-Effect Transistors. *J. Am. Chem. Soc.* **2009**, *131*, 9396–9404.
- (25) Chua, L.-L.; Zaumseil, J.; Chang, J.-F.; Ou, E. C.-W.; Ho, P. K.-H.; Sirringhaus, H.; Friend, R. H. General Observation of N-Type Field-Effect Behaviour in Organic Semiconductors. *Nature* **2005**, *434*, 194–199.
- (26) Sauvé, G.; Javier, A. E.; Zhang, R.; Liu, J.; Sydlik, S. A.; Kowalewski, T.; McCullough, R. D. Well-Defined, High Molecular Weight Poly(3-Alkylthiophene)s in Thin-Film Transistors: Side Chain Invariance in Field-Effect Mobility. *J. Mater. Chem.* **2010**, 20, 3195.
- (27) Fraštia, L'.; Archer, A. J.; Thiele, U. Modelling the Formation of Structured Deposits at Receding Contact Lines of Evaporating Solutions and Suspensions. *Soft Matter* **2012**, *8*, 11363.
- (28) Monteux, C.; Elmaallem, Y.; Narita, T.; Lequeux, F. Advancing-Drying Droplets of Polymer Solutions: Local Increase of the Viscosity at the Contact Line. *EPL Europhys. Lett.* **2008**, 83, No. 34005.
- (29) Diao, Y.; Zhou, Y.; Kurosawa, T.; Shaw, L.; Wang, C.; Park, S.; Guo, Y.; Reinspach, J. A.; Gu, K.; Gu, X.; Tee, B. C. K.; Pang, C.; Yan, H.; Zhao, D.; Toney, M. F.; Mannsfeld, S. C. B.; Bao, Z. Flow-Enhanced Solution Printing of All-Polymer Solar Cells. *Nat. Commun.* 2015, 6, No. 7955.
- (30) Orejon, D.; Sefiane, K.; Shanahan, M. E. R. Stick—Slip of Evaporating Droplets: Substrate Hydrophobicity and Nanoparticle Concentration. *Langmuir* **2011**, 27, 12834—12843.
- (31) Deegan, R. D.; Bakajin, O.; Dupont, T. F.; Huber, G.; Nagel, S. R.; Witten, T. A. Capillary flow as the Cause of Ring Stains from Dried Liquid Drops. *Nature* **1997**, *389*, 827–829.
- (32) Decker, E. L.; Garoff, S. Using Vibrational Noise to Probe Energy Barriers Producing Contact Angle Hysteresis. *Langmuir* **1996**, *12*, 2100–2110.
- (33) Marmur, A. Wetting on Real Surfaces. J. Imaging Sci. Technol. 2000, 44, 406–409.
- (34) Joanny, J. F.; de Gennes, P. G. A Model for Contact Angle Hysteresis. J. Chem. Phys. 1984, 81, 552-562.

- (35) Johnson, R. E.; Dettre, R. H.; Brandreth, D. A. Dynamic Contact Angles and Contact Angle Hysteresis. *J. Colloid Interface Sci.* 1977, 62, 205–212.
- (36) Decker, E. L.; Frank, B.; Suo, Y.; Garoff, S. Physics of Contact Angle Measurement. *Colloids Surf.*, A 1999, 156, 177–189.
- (37) Meiron, T. S.; Marmur, A.; Saguy, I. S. Contact Angle Measurement on Rough Surfaces. *J. Colloid Interface Sci.* **2004**, *274*, 637–644.
- (38) Eral, H. B.; 't Mannetje, D. J. C. M.; Oh, J. M. Contact Angle Hysteresis: A Review of Fundamentals and Applications. *Colloid Polym. Sci.* **2013**, 291, 247–260.
- (39) Stokes, J. P.; Higgins, M. J.; Kushnick, A. P.; Bhattacharya, S.; Robbins, M. O. Harmonic Generation as a Probe of Dissipation at a Moving Contact Line. *Phys. Rev. Lett.* **1990**, *65*, 1885.
- (40) Andrieu, C.; Sykes, C.; Brochard, F. Average Spreading Parameter on Heterogeneous Surfaces. *Langmuir* **1994**, *10*, 2077–2080.
- (41) Young, T., III An Essay on the Cohesion of Fluids. *Philos. Trans. R. Soc. London* **1805**, *95*, 65–87.
- (42) Rodríguez-Valverde, M. A.; Montes Ruiz-Cabello, F. J.; Cabrerizo-Vílchez, M. A. A New Method for Evaluating the Most-Stable Contact Angle Using Mechanical Vibration. *Soft Matter* **2011**, 7, 53–56.
- (43) Ruiz-Cabello, F. J. M.; Rodríguez-Valverde, M. A.; Cabrerizo-Vilchez, M. A New Method for Evaluating the Most Stable Contact Angle Using Tilting Plate Experiments. *Soft Matter* **2011**, *7*, 10457.
- (44) Montes Ruiz-Cabello, F. J.; Rodríguez-Valverde, M. A.; Cabrerizo-Vílchez, M. A. Comparison of the Relaxation of Sessile Drops Driven by Harmonic and Stochastic Mechanical Excitations. *Langmuir* **2011**, *27*, 8748–8752.
- (45) Volpe, C. D.; Maniglio, D.; Morra, M.; Siboni, S. The Determination of a 'Stable-Equilibrium' Contact Angle on Heterogeneous and Rough Surfaces. *Colloids Surf., A* **2002**, *206*, 47–67.
- (46) Giri, G.; Verploegen, E.; Mannsfeld, S. C. B.; Atahan-Evrenk, S.; Kim, D. H.; Lee, S. Y.; Becerril, H. A.; Aspuru-Guzik, A.; Toney, M. F.; Bao, Z. Tuning Charge Transport in Solution-Sheared Organic Semiconductors Using Lattice Strain. *Nature* **2011**, *480*, 504–508.
- (47) Larson, R. G. Transport and Deposition Patterns in Drying Sessile Droplets. *AIChE J.* **2014**, *60*, 1538–1571.
- (48) Mohammadi, E.; Zhao, C.; Meng, Y.; Qu, G.; Zhang, F.; Zhao, X.; Mei, J.; Zuo, J.-M.; Shukla, D.; Diao, Y. Dynamic-Template-Directed Multiscale Assembly for Large-Area Coating of Highly-Aligned Conjugated Polymer Thin Films. *Nat. Commun.* **2017**, 8, No. 16070.
- (49) Wu, D.; Kaplan, M.; Ro, H. W.; Engmann, S.; Fischer, D. A.; DeLongchamp, D. M.; Richter, L. J.; Gann, E.; Thomsen, L.; McNeill, C. R.; Zhang, X. Blade Coating Aligned, High-Performance, Semiconducting-Polymer Transistors. *Chem. Mater.* **2018**, 1924–1936
- (50) Chang, J.; Sonar, P.; Lin, Z.; Zhang, C.; Zhang, J.; Hao, Y.; Wu, J. Controlling Aggregation and Crystallization of Solution Processed Diketopyrrolopyrrole Based Polymer for High Performance Thin Film Transistors by Pre-Metered Slot Die Coating Process. *Org. Electron.* **2016**, *36*, 113–119.
- (51) Lin, F.-J.; Guo, C.; Chuang, W.-T.; Wang, C.-L.; Wang, Q.; Liu, H.; Hsu, C.-S.; Jiang, L. Directional Solution Coating by the Chinese Brush: A Facile Approach to Improving Molecular Alignment for High-Performance Polymer TFTs. *Adv. Mater.* **2017**, No. 1606987.
- (52) Matsumoto, T.; Ou-Yang, W.; Miyake, K.; Uemura, T.; Takeya, J. Study of Contact Resistance of High-Mobility Organic Transistors through Comparisons. *Org. Electron.* **2013**, *14*, 2590–2595.
- (53) Pesavento, P. V.; Puntambekar, K. P.; Frisbie, C. D.; McKeen, J. C.; Ruden, P. P. Film and Contact Resistance in Pentacene Thin-Film Transistors: Dependence on Film Thickness, Electrode Geometry, and Correlation with Hole Mobility. *J. Appl. Phys.* **2006**, *99*, No. 094504.
- (54) Richards, T. J.; Sirringhaus, H. Analysis of the Contact Resistance in Staggered, Top-Gate Organic Field-Effect Transistors. *J. Appl. Phys.* **2007**, *102*, No. 094510.

- (55) Yamamura, A.; Watanabe, S.; Uno, M.; Mitani, M.; Mitsui, C.; Tsurumi, J.; Isahaya, N.; Kanaoka, Y.; Okamoto, T.; Takeya, J. Wafer-Scale, Layer-Controlled Organic Single Crystals for High-Speed Circuit Operation. *Sci. Adv.* **2018**, *4*, No. eaao5758.
- (56) He, D.; Qiao, J.; Zhang, L.; Wang, J.; Lan, T.; Qian, J.; Li, Y.; Shi, Y.; Chai, Y.; Lan, W.; Ono, L. K.; Qi, Y.; Xu, J.-B.; Ji, W.; Wang, X. Ultrahigh Mobility and Efficient Charge Injection in Monolayer Organic Thin-Film Transistors on Boron Nitride. *Sci. Adv.* **2017**, 3, No. e1701186.
- (57) Rivnay, J.; Mannsfeld, S. C. B.; Miller, C. E.; Salleo, A.; Toney, M. F. Quantitative Determination of Organic Semiconductor Microstructure from the Molecular to Device Scale. *Chem. Rev.* **2012**, *112*, 5488–5519.
- (58) Sirringhaus, H.; Brown, P. J.; Friend, R. H.; Nielsen, M. M.; Bechgaard, K.; Langeveld-Voss, B. M. W.; Spiering, A. J. H.; Janssen, R. A. J.; Meijer, E. W.; Herwig, P.; de Leeuw, D. M. Two-Dimensional Charge Transport in Self-Organized, High-Mobility Conjugated Polymers. *Nature* **1999**, *401*, 685–688.
- (59) Bittle, E. G.; Basham, J. I.; Jackson, T. N.; Jurchescu, O. D.; Gundlach, D. J. Mobility Overestimation Due to Gated Contacts in Organic Field-Effect Transistors. *Nat. Commun.* **2016**, *7*, No. 10908.
- (60) Uemura, T.; Rolin, C.; Ke, T.-H.; Fesenko, P.; Genoe, J.; Heremans, P.; Takeya, J. On the Extraction of Charge Carrier Mobility in High-Mobility Organic Transistors. *Adv. Mater.* **2016**, 28, 151–155.
- (61) Choi, H. H.; Cho, K.; Frisbie, C. D.; Sirringhaus, H.; Podzorov, V. Critical Assessment of Charge Mobility Extraction in FETs. *Nat. Mater.* **2017**, *17*, *2*.
- (62) Haase, K.; Teixeira da Rocha, C.; Hauenstein, C.; Zheng, Y.; Hambsch, M.; Mannsfeld, S. C. B. High-Mobility, Solution-Processed Organic Field-Effect Transistors from C8-BTBT:Polystyrene Blends. *Adv. Electron. Mater.* **2018**, *4*, No. 1800076.
- (63) Teixeira da Rocha, C.; Haase, K.; Zheng, Y.; Löffler, M.; Hambsch, M.; Mannsfeld, S. C. B. Solution Coating of Small Molecule/Polymer Blends Enabling Ultralow Voltage and High-Mobility Organic Transistors. *Adv. Electron. Mater.* **2018**, No. 1800141.
- (64) Karthaus, O.; Gråsjö, L.; Maruyama, N.; Shimomura, M. Formation of Ordered Mesoscopic Polymer Arrays by Dewetting. *Chaos Interdiscip. J. Nonlinear Sci.* **1999**, *9*, 308–314.
- (65) Chen, Z.; Lee, M. J.; Shahid Ashraf, R.; Gu, Y.; Albert-Seifried, S.; Meedom Nielsen, M.; Schroeder, B.; Anthopoulos, T. D.; Heeney, M.; McCulloch, I.; Sirringhaus, H. High-Performance Ambipolar Diketopyrrolopyrrole-Thieno[3,2- b] Thiophene Copolymer Field-Effect Transistors with Balanced Hole and Electron Mobilities. *Adv. Mater.* 2012, 24, 647–652.
- (66) Yuan, Q.; Mannsfeld, S. C. B.; Tang, M. L.; Toney, M. F.; Lüning, J.; Bao, Z. Thin Film Structure of Tetraceno[2,3- b] Thiophene Characterized by Grazing Incidence X-Ray Scattering and Near-Edge X-Ray Absorption Fine Structure Analysis. *J. Am. Chem. Soc.* 2008, 130, 3502–3508.